Article:

Jet flame heights, lift-off distances, and mean flame surface density for extensive ranges of fuels and flow rates

Derek Bradley[a],*, Phil H. Gaskell[b], Xiaojun. Gu[c], Adriana Palacios[a,d]

[a]School of Mechanical Engineering, University of Leeds, Leeds LS2 9JT, UK.

[b]School of Engineering and Computing Sciences, Durham University, Durham DH1 3LE, UK.

[c]Department of Scientific Computing, STFC Daresbury Laboratory, Warrington WA4 4AD, UK.

[d] Department of Chemical, Food and Environmental Engineering, Fundacion Universidad de las Americas, Puebla, Puebla 72810, Mexico.

*Corresponding author. Fax: +44 113 242 4611. E-mail address: d.bradley@leeds.ac.uk

Abstract

An extensive review and re-thinking of jet flame heights and structure, extending into the choked/supersonic regime is presented, with discussion of the limitations of previous flame height correlations. Completely new dimensionless correlations for the plume heights, lift-off distances, and mean flame surface densities of atmospheric jet flames, in the absence of a cross wind, are presented. It was found that the same flow rate parameter could be used to correlate both plume heights and flame lift-off distances. These are related to the flame structure, jet flame instability, and flame extinction stretch rates, as revealed by complementary experiments and computational studies. The correlations are based on a vast experimental data base, covering 880 flame heights. They encompass pool fires and flares, as well as choked and unchoked jet flames of CH_4, C_2H_2, C_2H_4, C_3H_8, C_4H_{10} and H_2, over a wide range of conditions. Supply pressures range from 0.06 to 90 MPa, discharge diameters from $4 \cdot 10^{-4}$ to 1.32 m, and flame heights from 0.08 to 110 m. The computational studies enabled reaction zone volumes to be estimated, as a proportion of the plume volumes, measured from flame photographs, and temperature contours. This enabled mean flame surface densities to be estimated, together with mean volumetric heat releases rates. There is evidence of a "saturation" mean surface density and increases in turbulent burn rates being accomplished by near pro rata increases in the overall volume of reacting mixture.

Keywords: Jet flame height; Lift-off distance; Flamelet modelling; "Fracking"; Jet flame stability; Mean flame surface density

Nomenclature

A	surface area of fuel flow (m^2)
$\bar{c}$	mean reaction progress variable (0-1)
C_p	specific heat of fuel at constant pressure (but for Q* it is for the ambient air) (kJ/kg-K)
d	equivalent diameter of fire plume (m)
D	pipe diameter (m)
f	ratio of fuel to air moles in fuel-air mixture for maximum burning velocity, S_L
f_b	multiplying factor for S_L to express reduction in mean burning velocity below maximum S_L
f_v	fraction of plume volume in which reaction is occurring
Fr	Froude number (u^2/gD)
g	acceleration of gravity (m/s^2)
h	length of fire plume (m)
H	flame height, from top of burner or fire source diameter to flame tip (m)
I_o	dimensionless factor to allow for effect of flame stretch rate on S_L
k	reciprocal wave length for flame surface density (m^{-1})
K	Karlovitz stretch factor

l   integral length scale of turbulence (m)

L   flame lift-off distance (m)

P_a atmospheric pressure (Pa)

P_i initial stagnation pressure (Pa)

$\dot{Q}$ heat release rate (kW)

Q*   dimensionless parameter, Froude-like flame source characterisation

$$\left(Q* = \dot{Q} \big/ \rho_a C_p T_a \sqrt{gD} D^2 \right)$$

r   flame radius (mm)

r_m air to fuel mass ratio for stoichiometric mixture

R^2 correlation coefficient

R_l turbulent Reynolds number

R_λ turbulent Reynolds number on the Taylor scale

R_M momentum parameter defined in [61]

Re_L Reynolds number based on S_L and D, (DS_L/ν)

S_L maximum laminar burning velocity of the fuel-air mixture under conditions of ambient atmosphere (m/s)

T_a temperature of the ambient atmosphere (K)

T_b temperature of burned gas (K)

T_u temperature of unburned gas (K)

u   fuel flow mean velocity at the exit plane of pipe for subsonic flow. For ratios of atmospheric pressure to pipe pressure equal to, or less than, the critical pressure ratio, sonic velocity after isentropic expansion (m/s)

u_e fuel flow mean velocity at exit plane of pipe for subsonic flow. For ratios of atmospheric to pipe pressure less than, or equal to critical pressure ratio, sonic/supersonic velocity after isentropic expansion (m/s)

u_l laminar burning velocity (m/s)

u'   rms turbulent velocity (m/s)

U*   dimensionless flow number for choked and unchoked flow, $(u/S_L)Re_L^{-0.4}(P_i/P_a)$

x   axial position (mm)

Greek

α_m ratio of combined mass fuel and air that is burning, to that of fuel

δ laminar flame thickness, under conditions of ambient atmosphere (ν/S_L) and (ν/u_l) (m)

ΔH heat of combustion (kJ/kg)

γ ratio of specific heats

λ Taylor length scale (m)

ν kinematic viscosity, under conditions of ambient atmosphere (m^2/s)

ρ	density (kg/m^3)
ρ_a	density at pressure of ambient atmosphere of the ambient gas (air) (kg/m^3)
$\overline{\Sigma}$	mean flame surface density (m^{-1})

Subscripts

a	ambient conditions or air
e	with fuel isentropically expanded to pressure of ambient atmosphere
i	initial stagnation conditions
j	at outlet orifice (jet exit)

1. Introduction

In the study of jet flames, the jet is defined by a discharge from the pipe, and the flame by the reaction zone. The plume is the volume of hot gases, that is usually visible, and with an edge temperature of about 800K. The flame height is the distance from the pipe exit plane to the top of the plume. The commonly used term "jet flame height", can be misleading, in so far as it might suggest significant reaction at the top of the plume. Jet flames are important in a variety of contexts: they arise in the controlled flaring of flammable gases, the uncontrolled rupture of pipelines and containers, as well as in oil and gas field blow-outs. Jets are classified as flares when they are employed for the safe disposal of flammable gases from pipes with outlet diameters greater than 150 mm, in an environmentally compliant manner. Between 10% and 30% of their energy can be emitted as thermal radiation [1]. Cross winds can aggravate partial extinction and pollution. These are best countered by jets with high momentum [2]. Flaring of natural gases has recently increased significantly, with the growth of "fracking".

Jet flame size is of crucial importance, not only because of the possible consequent fire and damage, but also because, with an appropriate understanding, it can be used to quantify the magnitude of the discharge. A number of correlations have been proposed for both flame height and the lift-off distance of the base of the flame above the pipe exit plane. Many of the correlations have been limited to particular gases and operational regimes and might not be applicable for all gases under different circumstances.

The paper reports a comprehensive survey of all the known experimental data on the flame dimensions of controlled atmospheric jet flames. It covers six fuels, in flow regimes that range from small leakages and buoyant pool flames to turbulent subsonic and supersonic jets. A vast data bank has been compiled covering 880 sets of flame height measurements, from 0.08 to 110 m, and 740 sets of associated flame lift-off distances, including new measurements in the course of the present study. Upstream pressures ranged from 0.06 to 90 MPa, and discharge diameters from $4 \cdot 10^{-4}$ to 1.32 m.

The data bank is first used in the correlation of dimensionless flame heights in terms of the well-established dimensionless Q* group [3]. This is followed by their correlations in terms of a proposed new, more general, dimensionless flow number, U*, which is also shown to correlate flame lift-off distances. The new group is based on the physico-chemical parameters relevant to turbulent burning, including the Karlovitz stretch factor.

The group arises from stretched laminar flamelet, turbulence modelling [4-8] and from correlations of turbulent burning velocity [9,10].

The correlations of flame heights, combined with some measured plume volumes and mean diameters and computed reacting volumes enable estimates to be made of mean overall flame surface densities and mean volumetric heat release rates. These suggest the possible existence of a "saturation" value of mean overall flame surface density at sufficiently high turbulence.

2. Experimental data

Data have been extracted from 34 publications, ranging from the pioneering works of Hawthorne et al. [11], and Wohl et al. [12] in 1949, to the recent unique high altitude propane data of Hu et al. [13] and Wang et al. [14], collected in Lhasa at ambient pressures down to 60 kPa. The studies of hydrogen jet flames have involved inlet pipe pressures up to 90 MPa. The subsequent expansion to the pressure of the ambient atmosphere was assumed to be isentropic, with a non-ideal gas following the Abel-Noble equation of state [15-17]. In many cases the supply pipe pressure was close to atmospheric and the exit velocity close to that measured in the pipe. For ratios of atmospheric pressure to pipe pressure equal to, or less than, the critical pressure ratio, the exit velocity was assumed sonic after isentropic expansion.

Previous compilations and generalisations of measurements would typically embody about 25 data sets. The present set, involving flame heights and lift-off distances, is summarised in Table 1. It has involved extensive re-working of data from many sources, covering acetylene, butane, ethylene, hydrogen, methane and propane, in laminar and turbulent flames. The mode of release could be horizontal, but was principally vertical, into relatively still air, with wind speeds of less than 2 m/s. A variety of definitions and techniques for identifying and measuring flame boundaries can be found in the literature [11,23-28], with no single definition being generally preferred. Flame heights, H, have been measured, using various techniques, as the distance from the exit plane of the jet pipe, of diameter D, to the upper, variously detected, limits. The flame lift-off distance, L, was taken to be the distance between the exit plane and the base of the lifted flame, see Fig. 1.

3. Jet flame height correlations

3.1 The Q* parameter

Early analyses of buoyant flame plumes, from pool fires and wood cribs, employed a Froude number based upon the height, H, with $Fr = u^2/gH$, with u the upwards velocity, and g the acceleration due to gravity. Buoyant, abnormally high, fire plumes, as might be attained in warfare, wild fires, and other disasters, can induce high fire storm velocities at the base [29]. The situation is different with jet flames, and the practice was adopted of basing the Froude number on the pipe diameter, D, rather than H [30,31]. McCaffrey [3] expressed the heat release rate, $\dot{Q}$, in terms of the total mass flow rate of fuel, $Au\rho_j$ across the surface area of fuel flow, A, multiplied by its mass specific heat of reaction, ΔH. With $Fr = u^2/gD$ this yielded:

$$Fr = \left[\dot{Q}^2 \left(A^2 \Delta H^2 \rho_j^2 gD \right)^{-1} \right]. \tag{1}$$

Now $\Delta H = C_p(T_b - T_u)$, where C_p is the mean specific heat of the fuel at constant pressure, and, in which, the bracketed term is the temperature difference between burned and unburned gas. Zukoski [32] observed there was little change in $(T_b - T_u)$ with the different fuels, and this facilitated greater generalisation, by simply dimensionally expressing a temperature effect by T_u. Similarly, in dimensional terms, with a circular cross section of flow, A^2 might be expressed by D^4, with the result that $Fr^{1/2}$ is a function of $\left[\dot{Q}^2 \left(D^4 C_p^2 T_u^2 \rho_j^2 gD \right)^{-1} \right]^{1/2}$. Zukoski et al. [31] showed that this gave rise to the dimensionless group $Q*$, with:

$$Q* = \dot{Q}\left(C_p T_u \rho_j g^{1/2} D^{5/2} \right)^{-1} . \qquad (2)$$

The origins of the properties in Eqs. (1) and (2) lie in the fuel jet properties, but Zukoski [31] and McCaffrey [3] chose properties of the ambient air. This practice is followed in the present paper for all values of $Q*$. Other authors subsequently employed this same definition of $Q*$ to correlate the flame heights of pool fires [3,33,34]. McCaffrey pointed out that Zukoski, whose main concern was pool fires, took the lead in correlating his data in terms of $Q*$ [3]. McCaffrey showed it could be used outside the buoyancy and pool fire regimes to correlate H/D over surprisingly broad regimes, including turbulent jet flames. The original correlation was presented as logarithmic plots of H/D against $Q*^{2/5}$ [3] and employed the experimental data in [11,24,33,35-39].

Such a plot, but now employing the entire newly compiled data base, and showing different regimes, is shown in Fig. 2. It contains references to all the relevant data sources. The original correlation in [3] is extended to a maximum value of H/D of about 700, and one of $Q*$ of $13 \cdot 10^6$, with $Q*^{2/5} = 700.7$. It is shown on Fig. 2 by the bold curve. The maximum increase in H/D levelled off at somewhat different values for each group. Those of Becker and Liang's data correlation [35] are shown on the present figure, as $Q*$ attained $2 \cdot 10^7$.

The present data range beyond the original levelling-off, which probably marks the end of a sonic flow regime, followed by a resumed increase in H/D with $Q*^{2/5}$, in a supersonic regime. The newly compiled data bank suggests a transition regime that may include choked, subsonic and supersonic flows. Beyond this, at higher $Q*^{2/5}$, lies the third supersonic regime. Sometimes both choked and supersonic flames appeared in the "subsonic" regime, while subsonic flames appeared in the choked and supersonic regime. Mogi and Horiguchi [51], in their recent experimental study of hydrogen jet flames, found H/D values to be proportional to $Q*^{0.25}$ for values of $Q*$ up to $2 \cdot 10^8$.

Although algebraic correlations of H/D in terms of $Q*$ were presented in [3] for the separate contributors of data, there was no overall correlation equation. On the basis of the present data bank, the best fit lines for all the data on Fig. 2 are expressed by:

$$H/D = 3.4 Q*^{2/5} - 0.6 \quad \text{for } Q*^{2/5} < 100, \text{ in the subsonic regime;} \qquad (3)$$

$$H/D = 1.9 Q*^{2/5} \quad \text{for } Q*^{2/5} > 100, \text{ in the choked and supersonic regime.} \qquad (4)$$

The corresponding correlation coefficient, R^2, has values of 0.95 for both of these regimes.

Another approach is that of Heskestad [61] who, in 1999, also considered the high-momentum jet regime, based on an extension of his correlation for buoyancy-controlled turbulent diffusion flames. He suggested a momentum parameter, R_M, defined as the ratio of gas release momentum to that generated by a purely buoyant jet flame. For $R_M \geq 0.1$ and for many common gases, H/D in the momentum regime was found to depend in a simple manner on the air to fuel mass ratio for a stoichiometric mixture, r_m, and the source gas density at discharge [61,62]:

$$H/D = 18.5(\rho_j / \rho_a)^{1/2} r_m. \tag{5}$$

More recently, Molkov and Saffers [63] have employed an original dimensionless group accounting for both Froude and Reynolds number effects for hydrogen jet flames, but this did not provide a suitable correlation for all the fuels in the present data base.

3.2. The U* parameter

The analytical background to the Q* and some other dimensionless groups does not include combustion parameters, such as burning velocities, nor any characterisation of the turbulence. This is in contrast to the approach of Vanquickenborne and Van Tiggelen [40] and Kalghatgi [36], who balanced a turbulent burning velocity against the velocity of the oncoming gas. The latter also presented a dimensionless correlation for the lift-off distance that involves S_L, the maximum laminar burning velocity of the fuel-air mixture under atmospheric conditions.

The stretched laminar flamelet modelling of turbulent jet flames presented in [4-7,9] analysed the air entrainment and intense fuel/air mixing at the base of the flame in the lift-off volume. Even when localised flammable mixtures were created, the ratio of chemical, δ/u_l, to eddy, λ / u' lifetime that defines the Karlovitz stretch factor, K, was high enough to inhibit combustion, until the values relaxed further downstream. More formerly, u'/λ is the rms strain rate, in which λ is the Taylor scale. The turbulent Reynolds number on the Taylor scale is related to that on the integral length scale, l, by $R_\lambda = 4R_l^{0.5}$. The ratio yields [7]:

$$K = 0.25(u'/u_l)^2 R_l^{-0.5}, \tag{6}$$

in which R_l is the turbulent Reynolds number $= u'l/\nu$.

The model generated contours of mean volumetric heat release rate, mean mixture fraction, and mean strain rate, exemplified by the lifted flame in Fig. 3, as well as pdfs of localised premixed equivalence ratios. The last peaked at ratios close to unity.

Computed lift-off distances were correlated in terms of a dimensionless group related to K. In addition, measured turbulent burning velocities over a wide range of conditions, up to the development of flame extinctions, have been well correlated in terms of K and the strain rate Markstein number [10].

It was assumed that u' was proportional to u, measured at the pipe exit plane, and that the turbulent integral length scale, l, was proportional to D, also measured at the pipe exit plane. In addition, with u_l assumed close

to S_L, it readily can be shown that a simple dimensional grouping representative of the influence of K, or more precisely $K^{2/3}$, is $(u/S_L)Re_L^{-m}$, with m = 1/3, and $Re_L = S_L D/\nu$, a Reynolds number based on S_L and D. Whether such a dimensionless grouping might be used in correlations was tested using the present vast data bank of experimental flame heights, normalised by the pipe diameter. The results were encouraging and optimisation of the dimensionless relationships essentially involved optimising the value of m to obtain the highest value of the R^2 correlation coefficient. In addition, because jet pressures, P_i, were sometimes high, they were normalised by the atmospheric pressure, P_a and the associated pressure ratio was introduced into the relationship. These optimisations led to a value of m of 0.4 and a correlating jet flow parameter, U*, for the normalised flame heights, H/D, given by:

$$U^* = (u/S_L)Re_L^{-0.4}(P_i/P_a)_.$$ (7)

No influence of Markstein number was detected. This might be explained by both the near-stoichiometric premixing, at which Markstein numbers might all be fairly close to unity and the absence of sufficiently detailed data on jet flame blow out. Here, u is the mean velocity at the pipe exit plane. The values of maximum burning velocity, S_L, and ν in Re_L, are those for the ambient conditions. With a laminar flame thickness, $\delta = \nu/S_L$, Re_L becomes the pipe exit diameter expressed in laminar flame thicknesses, D/δ. The gaseous mixture kinematic viscosity, ν, under ambient conditions for the derivation of δ, was obtained from the software Gaseq [64].

Values of H/D from the data base are plotted against U* in Fig. 4. The key to the data point symbols is as given on Fig. 2. For $0 < H/D < 11$ in the pool fire regime, shown by the fainter curve demonstrate the exceptional additional effect of abnormally low temperature. Here, the fuel is liquid methane, at a temperature of 109K, significantly lower than that of 231K for liquid propane, which blends much better with the generalised relationship, excluding the low temperature methane data. Three distinct regimes can be identified. With increasing U*, these are: (i) a buoyancy-dominated laminar and pool flame regime that merges into a turbulent, subsonic regime; (ii) one of transition from momentum-dominated turbulent subsonic flames to (iii) one of choked, turbulent supersonic flames.

The best fit relationships of H/D, with U*, indicated by the bold curve, are:

$$H/D = 81U^{*0.46} \text{ for } U^* < 10, \text{ in the buoyancy and turbulent subsonic regimes;}$$ (8)

$$H/D = 230 \qquad \text{ for } 10 < U^* < 80, \text{ in the transition regime;}$$ (9)

$$H/D = 42U^{*0.4} \text{ for } U^* > 80, \text{ in the choked and turbulent supersonic regime.}$$ (10)

The corresponding R^2 correlation coefficients are all 0.96. The values for H/D in the transition regime is 230 ± 90.

4. Flame lift-off distance

4.1. Correlations of Kalghatgi et al.

Kalghatgi [36] measured vertical lift-off distances, L, from flame and schlieren images at the base of the flame, for burner diameters ranging from $1.08 \cdot 10^{-3}$ to $10.1 \cdot 10^{-3}$ m. An expression for this was embodied in another Reynolds number based on S_L, LS_L / ν_e, with ν_e the gas kinematic viscosity at the jet exit. This is also effectively L, normalised by the laminar flame thickness. Values were for the ambient conditions and are plotted against a flow parameter with some similarities to U*, namely (u_e/S_L) (ρ_e/ρ_a), but with no distance scale, with u_e the fuel flow mean velocity at the exit plane of the pipe for subsonic flow, and (ρ_e/ρ_a) the ratio of fuel density at the pressure of the ambient atmosphere, to that of the air at that pressure. For pressure ratios less than, or equal to, the critical value, Kalghatgi [36] assumed, as in [65], that the burner could be replaced by an equivalent convergent-divergent nozzle. Values of diameter, sonic/supersonic velocity, u_e, and density, ρ_e, were calculated on this basis for an assumed nozzle with isentropic expansion. This approach also was adopted, where necessary for the original and additional data in the current data bank, and are embodied in the correlation, with the results shown in Fig. 5. Originally, the density ratio at the exit plane, (ρ_e/ρ_a), was raised to a power of 1.5, but after further studies by Wu et al. [66,67] this power was changed to 1.0, as in Fig. 5.

On this figure, the data points from Hu, Wang, and co-workers [13,14] are for an ambient atmospheric pressure of about 60 kPa, with the jet discharging into large halls located in Lhasa and Hefei. The separated upper results from [13] and [14] on Fig. 5 are those which were taken at the very low atmospheric pressures that exist at altitude in Lhasa.

Data from these workers at the more normal atmospheric pressures followed the general correlation more closely. The greater lift-off distances in the Lhasa experiments can be explained by the reduced density of the air. For a given value of fuel jet velocity, u_e, discharging into the ambient air at a significantly lower pressure, the reduced surrounding air pressure results in less mass entrainment of air into the fuel jet and, consequently, this necessitated a greater lift-off distance for sufficient air entrainment to react the fuel. Figure 5 is the first such plot of choked jet flames for several fuels. The best curve fit to Kalghatgi's correlation, excluding the data from [13,14], is given by:

$$(LS_L / \nu_e) = 52.4 \left[(u_e/S_L)(\rho_e/\rho_a) - 11.8 \right]^{1.04}, \tag{11}$$

with an R^2 correlation coefficient of 0.97. This is the equation of the bold curve in Fig 5.

At values of dimensionless flow rate, (u_e/S_L) (ρ_e/ρ_a), below 20, the value of LS_L/ν_e, becomes small, and eventually zero, with the flame anchoring on the pipe, from which it can also readily lift off. The higher sonic flow rates lead into the supersonic regime.

4.2. The U* correlation

It was never proposed that the Q* group was suited to correlating lift-off distance. This is not surprising, bearing in mind the absence, within it, of combustion parameters. Nevertheless, trial attempts were made to correlate L/D with Q* using the present data bank. These were unsuccessful, with each fuel giving a very different relationship, demonstrating that the group was unable to capture the complexities of lift-off.

The computed streamlines in Fig. 3(a) show the importance of the inward air flow at the base of a lifted flame. The relative ratio of air to fuel flow depends upon the fuel, and is notably different in the case of hydrogen, compared with hydrocarbons. Hydrogen requires less air, with a consequent decrease in lift-off distance. With

due allowance for this dilution effect, the possibility that normalised lift-off distances, in addition to flame heights, might also be correlated with U* is explored. The differing air requirements necessitate the introduction of a multiplying factor, f, the ratio of fuel to air moles in the fuel-air mixture for the maximum S_L, in correlating the lift-off distance.

Figure 6 shows the experimental values of $(L/D)f^n$, plotted against U*. As with the height correlation, for all pressure ratios less than the critical value, u was taken to be the sonic velocity after isentropic expansion. At values of U* below 5 the lift-off distance becomes small and eventually zero, with the flame anchoring on the pipe as a diffusion flame, with $(L/D)f^n = 0$. It can then subsequently lift-off in an unstable regime. The optimal correlations shown on Fig. 6 are expressed by:

$$(L/D)f = 0.11U*-0.2 \text{ in the subsonic regime;} \tag{12}$$

$$(L/D)f^{0.2} = -54 + 17\ln(U*-23) \text{ in the choked and supersonic regimes;} \tag{13}$$

with the exponent for f being different for the two regimes.

Although the measured lift-off distances in the rarefied atmosphere of [13,14] in Fig. 5 are now better correlated, overall, the correlation expressions are less consistent than those for H/D, with R^2 values correspondingly 0.73 for the subsonic, and 0.71 for the choked and supersonic regimes. This reflects the high sensitivity of lift-off distances to the mixing processes and unstable flame fluctuations. No allowance was made for the differing air requirements in the expressions for plume height, Eqs. (8) to (10). However, on Fig. 4, values of H/D from [13,14], at the reduced ambient pressures, were 21% higher at a given U* than those at the more normal pressures.

5. Jet plume volume and mean overall flame surface density

An attempt was made to estimate the plume volume that was reacting and the associated mean overall flame surface density $\overline{\Sigma}$. The former involved careful jet flame measurements of thermocouple temperatures and infra-red emission intensities, of the type reproduced in Fig. 1, in [28], and the latter computations to reveal the extent of the reaction zone. The thermocouple measurements suggested the plume edges to lie at temperatures close to 800K. In Fig. 1 h is the length of the radiant emitting plume. The diameters were measured at different heights, squared, and integrated along the length of the image, to obtain the jet flame total volume. This was conveniently expressed by an equivalent diameter, d, of a cylinder of the same length and volume. The measured values of h/d are represented by the cross and semi-filled symbols, as a function of U*, in Fig. 7. The measurements, in methane and propane plumes extended over three regimes of U*, between 6 and 250, over which range the change in h/d is less than that in H/D.

The mass burning rate equation balances the mass flow rate of the fuel and air into the reaction zone with the mass burning rate there at the flame surface. In terms of the mean overall flame surface density, this gives:

$$\left(\pi D^2/4\right)\alpha_m u\rho_j = \overline{\Sigma}I_o\left(f_v h\pi d^2/4\right)f_b S_L\rho_a. \tag{14}$$

Here, α_m is the ratio of the total mass of the combined mass of fuel and air that is burning, to that of the fuel, and I_o expresses the effect of flame stretch rate on the burning velocity. This is 1 in the absence of flame

stretch rate effects, > 1 for negative, and < 1, for positive Markstein numbers. The fraction of the plume volume in which reaction is occurring is f_v, and f_b is a multiplying factor for S_L, estimated from the pdfs of equivalence ratios, to account for the reduction in mean burning velocity below the maximum, S_L. The computational detail required to obtain f_v, f_b, and $\bar{\Sigma}$ will be apparent from Fig. 3. With $\rho_j / \rho_a = (P_j / P_a)^{1/\gamma}$ and both sides of Eq. (14) multiplied by $\delta = \nu / S_L$:

$$\left(u/S_L\right)^{1/2} \mathrm{Re_L}^{-1/2} \left(P_j / P_a\right)^{1/2\gamma} \left(D/d\right)^{3/2} \left(d/h\right)^{1/2} = \left(\bar{\Sigma} \delta f_b I_o f_v / \alpha_m\right)^{1/2} . \tag{15}$$

It readily can be shown that:

$$U * \mathrm{Re_L}^{-0.6} \left(P_a / P_i\right)^{(\gamma-1)/\gamma} \left(D/d\right)^3 \left(d/h\right) = \bar{\Sigma} \delta f_b I_o f_v / \alpha_m , \tag{16}$$

which enabled $\bar{\Sigma} \delta$ to be found.

To estimate f_v, the fraction of the total plume volume supporting reaction, the computed spatially distributed volumetric heat release rate was integrated around the outer contour where the heat release rate began, to find the reaction zone volume. For propane, the necessary computational data were only available for $U* = 220$. The mean overall equivalence ratio of 0.75 gave $f_v = 0.29$, $\alpha_m = 21.8$, $f_b = 0.61$ and $I_o = 0.7$ [6]. The experimental detail for the methane flames were obtained from [48,71,72]. Other sources of data for the derivation of $\bar{\Sigma} \delta$ are given in Table 2. Values of $\bar{\Sigma} \delta$ are plotted by the open symbols against $U*$ in Fig. 7. Despite the dearth of computed data between $U* = 17.5$ and 220, the available data suggest a near constant value of $\bar{\Sigma} \delta = 0.008 \pm 0.002$.

Experiments and direct numerical simulations show the flame surface density can be expressed as a function of the mean reaction progress variable, $\bar{c}$, by $k\bar{c}(1-\bar{c})$ [73]. In this expression, the constant, k, is a reciprocal wave length indicative of the spatial changes in $\bar{c}$. A larger value of k would represent a smaller wave length, with increased surface wrinkling [74]. The equation is valid for values of $\bar{c}$ from 0.2 to 0.8. Above and below this range, values are anomalous and reflect the difficulty of defining the spatial limits of combustion. An appropriate spatial distribution for $\bar{c}$ enables its values to be expressed in spatial coordinates. With the simplifying assumption that between these limits of $\bar{c}$ its values increase linearly with gaseous volume, the mean overall flame surface density, $\bar{\Sigma}$, is 0.22k. For $\bar{\Sigma} \delta = 0.008 \pm 0.002$, it follows that $k\delta = 0.036 \pm 0.01$. The latter is close to the value of 0.05 ± 0.012, measured by different researchers in premixed turbulent flames [75]. With k a reciprocal wave length, $(k\delta)^{-1}$ is that wave length measured in unstretched laminar flame thicknesses. For $k\delta = 0.036$ the dimensionless wavelength is 27.8.

6. Discussion

The newly derived turbulent jet flame dimensionless flow number, $U*$ has been shown to be a capable parameter for the correlation of both appropriate dimensionless plume heights and jet flame lift-off distances over four flow regimes, buoyancy, subsonic flow, transition, choked and supersonic flow, and with a broad range of fuels. Provided there are no large differences in S_L for the different fuels, the $Q*$ group also gives

good correlations of plume heights. However, its lack of any distinctly combustion parameters or means of expressing the interplay of turbulent and chemical lifetimes render it unsuitable for predicting flame lift-off distances. On Fig. 5, at a given value of (u_e/S_L) (ρ_e/ρ_a) on the x axis, the value of LS_L/ν_e, on the y axis in the rarefied atmosphere were 84% greater than in the more normal atmospheres. The better correlation of these data points on Fig. 6 arises from changes in both x and y values. On the y axis, this involved allowance for the differing air requirements, while on the x axis the introduction of both a length scale parameter on Fig. 6, absent on Fig. 5, together with a greater sensitivity to pressure than to the ambient pressure on Fig. 5. As a result, on Fig. 6, the variation of the rarefied pressure points is shown in red, and is close to the mean values.

Kalghatgi's correlating parameters give good predictions of flame lift-off distances. The only exception being the Tibetan jet flames in rarified atmospheres. The (u_e/S_L) (ρ_e/ρ_a) group on the x axis of Fig. 5 does not uniquely define the flow rate of the fuel. The lift-off distance group, (LS_L/ν_e), reflects the amount of air required by the fuel. The atmospheric pressures for the data points of [13,14] were significantly less than the usual band of values. This suggests that their higher values of (LS_L/ν_e) arose from the more rarefied air supply. The difficulties in correlating lift-off distances are not surprising, bearing in mind the exacting mathematical modelling required for the complex chemical kinetics, coupled with very intense turbulence and shear rates with flame extinctions make it a very severe modelling test [76]. The sharp fall in dimensionless lift-off distance at the lower flow rate parameters in Figs. 5 and 6, are important indicators of potential jet flame instabilities.

A fall in flow rate can result in a stable laminar diffusion flame becoming anchored to the rim of the fuel pipe. A small, subsequent, increase in velocity can increase the flame stretch rate and extinguish the diffusion flame locally, with blow-off from the burner rim [12]. The fuel and air beneath the burned products can mix and be ignited by the hot products. The resulting mini-explosion creates a downward component of velocity, with the flame re-attaching on the burner rim, only for the fuel velocity to re-initiate the cycle. In this way, small changes in fuel velocity can generate relatively large lift-off oscillations.

With regard to the mean overall flame surface density, despite a number of measurement and computational uncertainties, values of $\overline{\Sigma}\delta$ for the propane and methane flames, in the range of U* from 6.8 to 220, hardly changed from $\overline{\Sigma}\delta = 0.008 \pm 0.002$. This approximates the mean fractional volume of the gas that is reacting within the overall reaction zone. For the propane jet flame, the associated mean volumetric heat release rate in the reaction zone was 170 MW/m^3. Values of $\overline{\Sigma}\delta$ have been observed for premixed turbulent flames, with rather similar "saturation" values of $\overline{\Sigma}\delta = 0.006 \pm 0.004$ [75]. A near constant "saturated" reacting volume of $\overline{\Sigma}\delta$ implies increases in burning rate are achieved, largely by an increase in the overall volume of the reacting mixture. It is interesting to speculate why this might be so.

One explanation is that an upper limit to flame wrinkling is attained by close volumetric packing of the flame front. Under such high curvature of the folds the stretch rate might critically affect the burn rate, perhaps even initiating fracture of the front. There is evidence of the dominating effect of small scale curvature from the 3D temporally-resolved measurements of turbulence-of flame interactions [77]. These demonstrate the details of

flame surface wrinkling by intertwined vortical structures. An interesting aspect of the product $k\delta$ arises, because the value of k represents a reciprocal wavelength for the changes in $\bar{c}$. Hence the reciprocal of $k\delta = 0.036$, namely, 28, also represents a limiting value of this wave length, expressed in terms of the laminar flame thickness.

7. Conclusions

1. A new comprehensive data bank of experimental jet flame heights and flame lift-off distances has been compiled, covering six fuels and different flow regimes.

2. The correlation of H/D with Q* has been extended to higher values of Q*, and shows a further increase in H/D in a supersonic regime, beyond the previously observed plateau.

3. Based on extensive mathematical modelling and experiments on turbulent flames, a new U* parameter has been formulated that gives improved, and more comprehensive, correlations for both fire plume height and flame lift-off distance. The latter identifies a regime of flame instabilities, comprising flame blow-offs and re-attachments.

4. Computer modelling and measuring of turbulent jet flames suggested that the overall reaction zone comprised between about 13 and 29% of the measured jet volume. From the model and measurements, it was possible to estimate the product of the overall mean flame surface density and laminar flame thickness, $\bar{\Sigma}\delta$ and $k\delta$.

5. Values of $\bar{\Sigma}\delta$ were in the region of 0.008 ± 0.002. This can be compared with similar measured values, in the region of 0.006 ± 0.004, for initially completely premixed turbulent flames. It suggests that, for a given mixture, turbulent burning rates are increased predominantly by an approximate, pro rata, increase in the overall volume of the reacting mixture. The value of $(k\delta)^{-1}$ suggests a limiting wave length for $\bar{c}$ of 28 laminar flame thicknesses.

6. These factors and the values of $\bar{\Sigma}\delta$, suggest a "saturation" packing of a highly folded flame, subjected to strong curvature stretch rates.

References

1. G.A. Chamberlain, Chem. Eng. Res. Des. 65 (1987) 299-309.
2. T.A. Brzustowski, Prog. Energy Combust. Sci. 2 (3) (1976) 129-141.
3. B. McCaffrey, in: P.J. DiNenno (Ed.), SFPE Fire Protection Handbook, Chapter 1–18: Flame Height, first ed., National Fire Protection Association, Quincy, MA, 02269, 1988, pp. 1–298-1–305.
4. D. Bradley, P.H. Gaskell, X.J. Gu, Proc. Combust. Inst. 27 (1998) 849-856.
5. D. Bradley, P.H. Gaskell, X.J. Gu, Proc. Combust. Inst. 27 (1998) 1199-1206.

6. A. Üngüt, D. Bradley, P.H. Gaskell, X.J. Gu, in: D. Bradley, D. Drysdale, G. Makhviladze (Eds.), Flamelet simulation of a large propane jet fire and its radiative emission, Proceedings Third International Seminar on Fire and Explosion Hazards, ISBN 1 9019 22170, University of Central Lancashire, Preston, U.K., 2001, p.443-452.

7. D. Bradley, M. Lawes, M.S. Mansour, Combust. Flame 158 (2011) 123-138.

8. D. Bradley, P.H. Gaskell, X.J. Gu, A. Sedaghat, Combust. Flame 143 (2005) 227-245.

9. D. Bradley, D.R. Emerson, P.H. Gaskell, X.J. Gu, Proc. Combust. Inst. 29 (2002) 2155-2162.

10. D. Bradley, M. Lawes, K. Liu, M.S. Mansour, Proc. Combust. Inst. 34 (2013) 1519-1526.

11. W.R. Hawthorne, D.S. Weddell, H.C. Hottel, Proc. Combust. Flame Expl. Phenomena 3 (1949) 266-288.

12. K. Wohl, C. Gazley, N. Kapp, Proc. Combust. Flame Expl. Phenomena 3 (1949) 288-300.

13. L. Hu, Q. Wang, M. Delichatsios, F. Tang, S. Zhang, L. Shouxiang, Fuel 109 (2013) 234-240.

14. Q. Wang, L. Hu, M. Zhang, F. Tang, X. Zhang, S. Lu, Combust. Flame 161 (2014) 1125-1130.

15. R.W. Schefer, W.G. Houf, T.C. Williams, B. Bourne, J. Colton, Int. J Hydrogen Energy 32 (12) (2007) 2081-2093.

16. V.V. Molkov, Fundamentals of Hydrogen Safety Engineering, Fourth European Summer School on Hydrogen Safety ESSHS, The Commission of the European Communities, Corsica, France, 2009, p. 107.

17. D. Bradley, J. Casal, A. Palacios, in: D. Bradley, G. Makhviladze, V. Molkov. (Eds.), Correlation of the Height of Turbulent Choked Jet Flames, Fire and Explosions Hazards Proceedings of the Sixth International Seminar on Fire and Explosions Hazards, University of Leeds, Leeds, U.K., 2010, pp. 255-266.

18. C.J. Sun, C.J. Sung, L. He, C.K. Law, Combust. Flame 118 (1999) 108-128.

19. C.M. Vagelopoulos, F.N. Egolfopoulos, C.K. Law, Proc. Combust. Inst. 25 (1994) 1341-1347.

20. F.N. Egolfopoulos, D.L. Zhu, C.K. Law, Proc. Combust. Inst. 23 (1990) 471-478.

21. K. Kumar, G. Mittal, C.J. Sung, C.K. Law, Combust. Flame 153 (2008) 343-354.

22. S.G. Davis, C.K. Law, Combust. Sci. Technol. 140 (1-6) (1998) 427-449.

23. F.R. Steward, Combust. Flame 3 (8) (1964) 171-178.

24. F.R. Steward, Combust. Sci. Technol. 2 (1970) 203-212.

25. T.A. Brzustowski, Combust. Sci. Technol. 6 (1973) 313-319.

26. E. Odgaard, Characteristics of Hydrocarbon Fires in Open-Air, Det Norske Veritas. Research Division Report No. 82-0704, Hoevik, Norway, 1983, p. 104.

27. R.W. Schefer, W.G. Houf, B. Bourne, J. Colton, Int. J Hydrogen Energy 31 (10) (2006) 1332-1340.

28. A. Palacios, J. Casal, Fuel 90 (2) (2011) 824-833.

29. D. Bradley, M. Lawes, G.M. Makhviladze, A. Palacios, in: D. Bradley, G. Makhviladze, V. Molkov, P. Sunderland, F. Tamanini (Eds.), Proc. of the Seventh International Seminar on Fire and Explosion Hazards (ISFEH7), University of Maryland, USA, 2013, pp. 666-675.

30. E.E. Zukoski, Convective Flows Associated with Room Fires, Semi-annual Progress Report to National Science Foundation, Grant No. GI 31892X1, California Institute of Technology, Washington, D.C., 1975, p. 57.

31. E.E. Zukoski, T. Kubota, B. Cetegen, Fire Saf. J. 3 (1980/1) 107-121.

32. E.E. Zukoski, in: G. Cox (Ed.), Combustion Fundamentals of Fire, Academic Press, San Diego, Calif., 1995, p. 476.

33. G. Cox, R. Chitty, Combust. Flame 60 (3) (1985) 219-232.

34. Y. Hasemi, M. Nishihata, Fire Sci. Technol. 7 (1987) 27-34.

35. H.A. Becker, D. Liang, Combust. Flame 32 (1978) 115-137.

36. G.T. Kalghatgi, Combust. Sci. Technol. 41 (1984) 17-29.

37. E.E. Zukoski, Proceedings of the First International Symposium on Fire Safety Science, Hemisphere, Fluid Dynamic Aspects of Room Fires, Fire Safety Science, New York, 1984, pp. 1-32.

38. P.H. Thomas, Proc. Com. Inst. 9 (1963) 844-859.

39. G. Heskestad, Fire Safety J. 5 (1983) 103-108.

40. L. Vanquickenborne, A. Van Tiggelen, Combust. Flame 10 (1966) 59-69.

41. G.G. Shevyakov, V.F. Komov, Combust. Expl. Shock Waves 13 (5) (1977) 563-566.

42. H.A. Becker, S. Yamazaki, Combust. Flame 33 (1978) 123-149.

43. B.J. McCaffrey, Some Measurements of the Radiative Power Output of Diffusion Flames, WSS Combustion Meeting Paper No. WSS/CI 81-15, Pullman (1981) p. 24.

44. F.C. Lockwood, H.A. Moneib, Combust. Flame 47 (1982) 291-314.

45. B.J. McCaffrey, D.D. Evans, Proc. Combust. Inst. 21 (1986) 25-31.

46. N.A. Rokke, J.E. Hustad, O.K. Sonju, Combust. Flame 97 (1) (1994) 88-106.

47. T.S. Cheng, C.R. Chiou, Combust. Sci. Technol. 136 (1998) 81-94.

48. M. Costa, C. Parente, A. Santos, Exp. Therm. Fluid Sci. 28 (2004) 729-734.

49. A. Santos, M. Costa, Combust. Flame 142 (2005) 160-169.

50. A.S. Langman, G.J. Nathan, J. Mi, P.J. Ashman, Proc. Combust. Inst. 31 (2007) 1599-1607.

51. T. Mogi, S. Horiguchi, J. Loss Prev. Process Indt. 22 (2009) 45-51.

52. A. Palacios, M. Muñoz, J. Casal, AIChE J. 55 (1) (2009) 256-263.

53. O. Sugawa, K. Sakai, Fire Sci. Technol. 17 (1997) 55-63.

54. T. Imamura, S. Hamada, T. Mogi, Y. Wada, S. Horiguchi, A. Miyake, T. Ogawa, Int. J Hydrogen Energy 33 (2008) 3426-3435.

55. E. Studer, D. Jamois, S. Jallais, G. Leroy, J. Hebrard, V. Blanchetiere, Int. J Hydrogen Energy 34 (2009) 9611-9619.

56. C. Proust, D. Jamois, E. Studer, Int. J Hydrogen Energy 36 (2011) 2367-2373.

57. E.S. Fishburne, H.S. Pergament, Proc. Combust. Inst. 17 (1979) 1063-1073.

58. A.D. Johnson, H.M. Brightwell, A.J. Carsley, Trans. IChemE 72 (B) (1994) 157-166.

59. A.S. Langman, G.J. Nathan, Exp. Therm. Fluid Sci. 35 (2011) 199-210.

60. E.E. Zukoski, B.M. Cetegen, T. Kubota, Proc. Combust. Inst. 20 (1984) 361-366.

61. G. Heskestad, Combust. Flame 118 (1999) 51-60.

62. G. Heskestad, in: P.J. DiNenno (Ed.), SFPE Fire Protection Handbook, Chapter 2–1: Fire Plumes, Flame Height, and Air Entrainment, fourth ed., National Fire Protection Association, Quincy, MA, 02269, 2008, pp. 2–1-2–20.

63. V. Molkov, J.B. Saffers, Int. J Hydrogen Energy 38 (19) (2013) 8141-8158.

64. C. Morley, Gaseq Chemical Equilibrium Program. c.morley@ukgateway.net.

65. Y.M. Annushkin, E.D. Sverdlov, Combust. Expl. Shock Waves 14 (5) (1978) 597-605.

66. Y. Wu, I.S. Al-Rahbi, Y. Lu, G.T. Kalghatgi, Fuel 86 (2007) 1840-1848.

67. Y. Wu, Y. Lu, I.S. Al-Rahbi, G.T. Kalghatgi, Int. J Hydrogen Energy 34 (2009) 5940-5945.

68. S. Donnerhack, N. Peters, Combust. Sci. Technol. 41 (1984) 101-108.

69. M.S. Cha, S.H. Chung, Proc. Combust. Inst. 26 (1996) 121-128.

70. C.O. Iyogun, M. Birouk, Combust. Sci. Technol. 180 (2008) 2186-2209.

71. T. Mahmud, S.K. Sangha, M. Costa, A. Santos, Fuel 86 (2007) 793-806.

72. L. Hu, X. Zhang, Q. Wang, A. Palacios, Fuel 150 (2015) 278-287.

73. D. Bradley, M. Lawes, M.S. Mansour, Proc. Combust. Inst. 32 (2009) 1587-1593.

74. A. Bagdanavicius, P.J. Bowen, D. Bradley, M. Lawes, M.S. Mansour, Submitted to Combustion and Flame, February 2015.

75. D. Bradley, M. Lawes, M.S. Mansour, Flow Turbulence Combust. 87 (2011) 191-204.

76. N. Peters, Turbulent Combustion, Cambridge University Press, U.K., 2000.

77. A.M. Steinberg, J.F. Driscoll, S.L. Ceccio, Exp. Fluids. 47 (2009) 527-547.

Tables

Table 1
Parameter range and fuel types spanning the present flame height and lift-off distance correlations.

Fuel	S_L, m·s^{-1}	Flame Height Measurements			Flame Lift-off Measurements		
		P_i, MPa	D, mm	H, m	P_i, MPa	D, mm	L, m
H_2	3.07 [18]	0.1-90	0.4-680	0.1-110	0.1-0.9	0.55-6.10	0.002-0.06
CH_4	0.39 [19]	0.1-3.47	1.9-500	0.34-31.6	0.1-0.31	1-152	0.01-7.15
C_2H_2	1.57 [20]	0.1-0.11	3.18	0.56-0.6	0.1-0.11	3.18	0.03-0.05
C_2H_4	0.72 [21]	0.1-0.11	5-8	0.8-1.45	0.1-0.13	4.06-8.3	0.005-0.14
C_3H_8	0.41 [19]	0.1-0.64	2-1320	0.08-12.7	0.1-0.64	0.84-43.1	0.006-1.2
	0.49 [18]	0.06-0.11	4-10	0.19-1.1	0.06-0.11	4-6	0.01-0.1
C_4H_{10}	0.41 [22]	0.1	10.16	0.22-1.2	-	-	-

Table 2
Data for the derivation of values of $(\overline{\Sigma}\delta)$ and $(k\delta)$ for methane and propane flames.

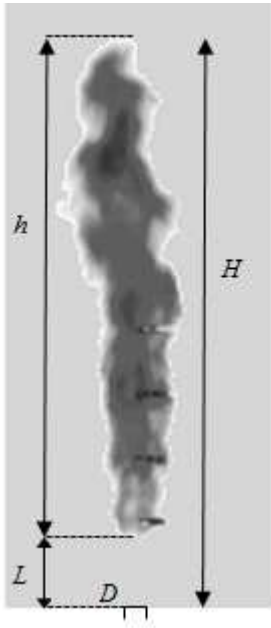| Fuel	Methane					Propane
Experiment	Present Work				[48]	[6]
D (mm)	6 [72]	5 [72]	5 [72]	5 [72]	5 [48]	17.8 [6]
h (m)	0.81 [72]	0.67 [72]	0.64 [72]	0.63 [72]	0.96 [48]	7.44 [6]
u (m/s)	20 [72]	28 [72]	31 [72]	35 [72]	46 [48]	256.4 [6]
d (m)	0.055	0.068	0.072	0.069	0.075 [71]	0.288
δ (m)	$4.1\cdot10^{-5}$	$4.1\cdot10^{-5}$	$4.1\cdot10^{-5}$	$4.1\cdot10^{-5}$	$4.1\cdot10^{-5}$	$3.6\cdot10^{-5}$
U^*	6.8	10	12	13	17.5	220
α_m	27.34	23.53	23.53	23.53	25.82	21.8
f_b	0.9	0.61	0.61	0.61	0.8	0.61
I_o	1	0.7	0.7	0.7	0.9	0.7 [6]
f_v	0.13	0.17	0.18	0.17	0.13	0.29 [6]
$\overline{\Sigma}\delta$	0.0071	0.0074	0.0078	0.010	0.0063	0.00854
$k\delta$	0.032	0.034	0.035	0.046	0.029	0.039

Figures

Figure 1. Infra-red image [28] of a propane jet flame, flame height, H, the lift-off distance, L, length of radiant emitting plume, h, and pipe exit plane, diameter D.

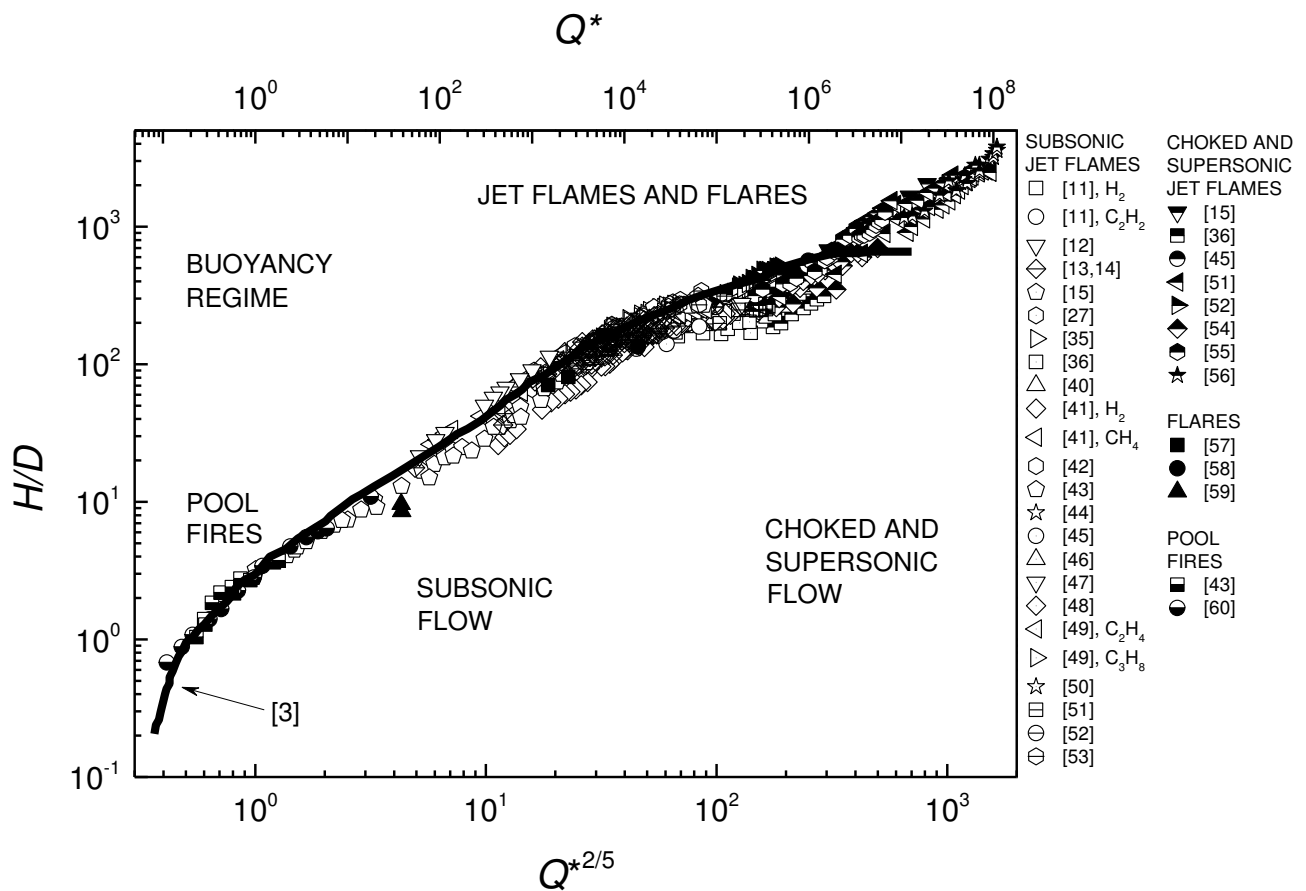
Figure 2. Normalised flame height, H/D, as a function of $Q^{*2/5}$, from present data bank. Original correlation of McCaffrey [3] shown by bold curve. This terminates at $Q^* = 13\cdot10^6$.
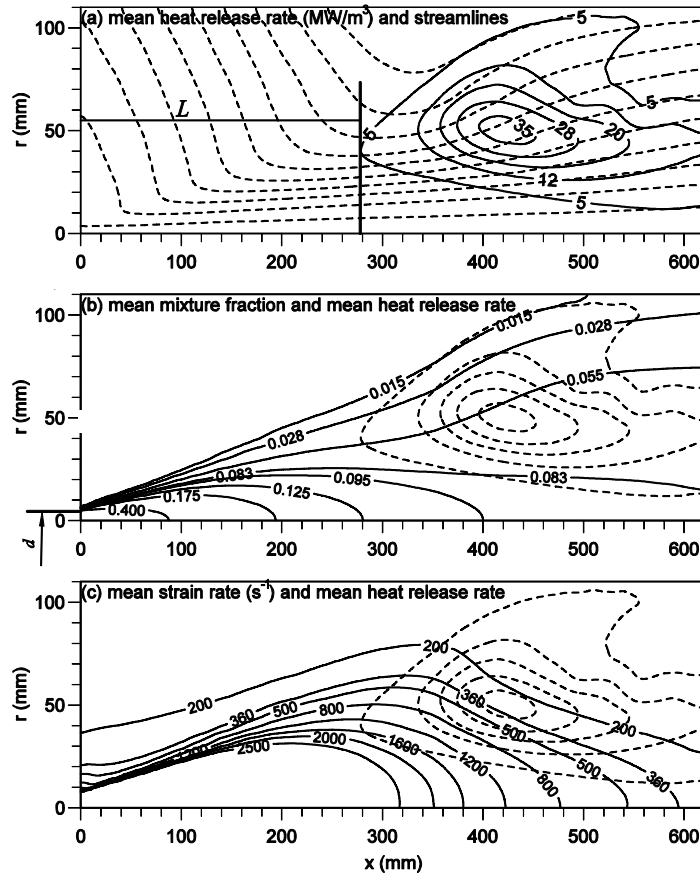
Figure 3. Location of mean volumetric heat release rate, related to (a) streamlines, (b) contours of mean mixture fraction, and (c) mean strain rate, s^{-1}, u = 100 m/s and D = 9 mm. From [5]. The pipe diameter, D, is shown as d in the figure.
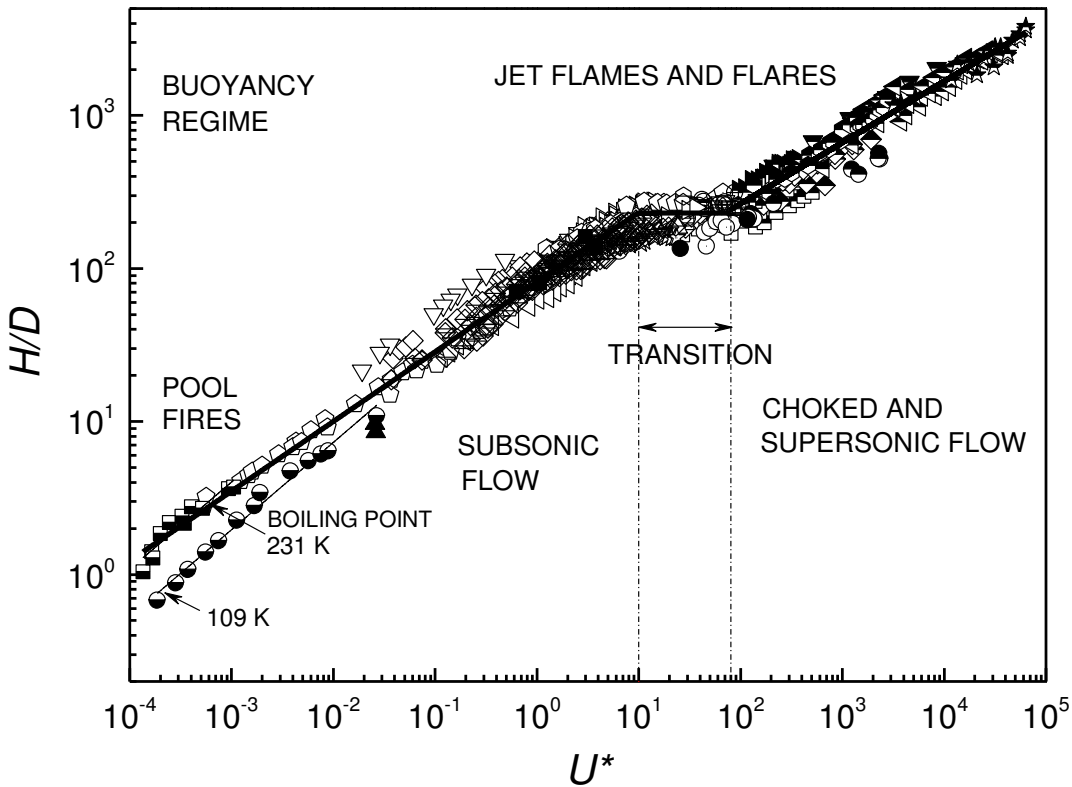

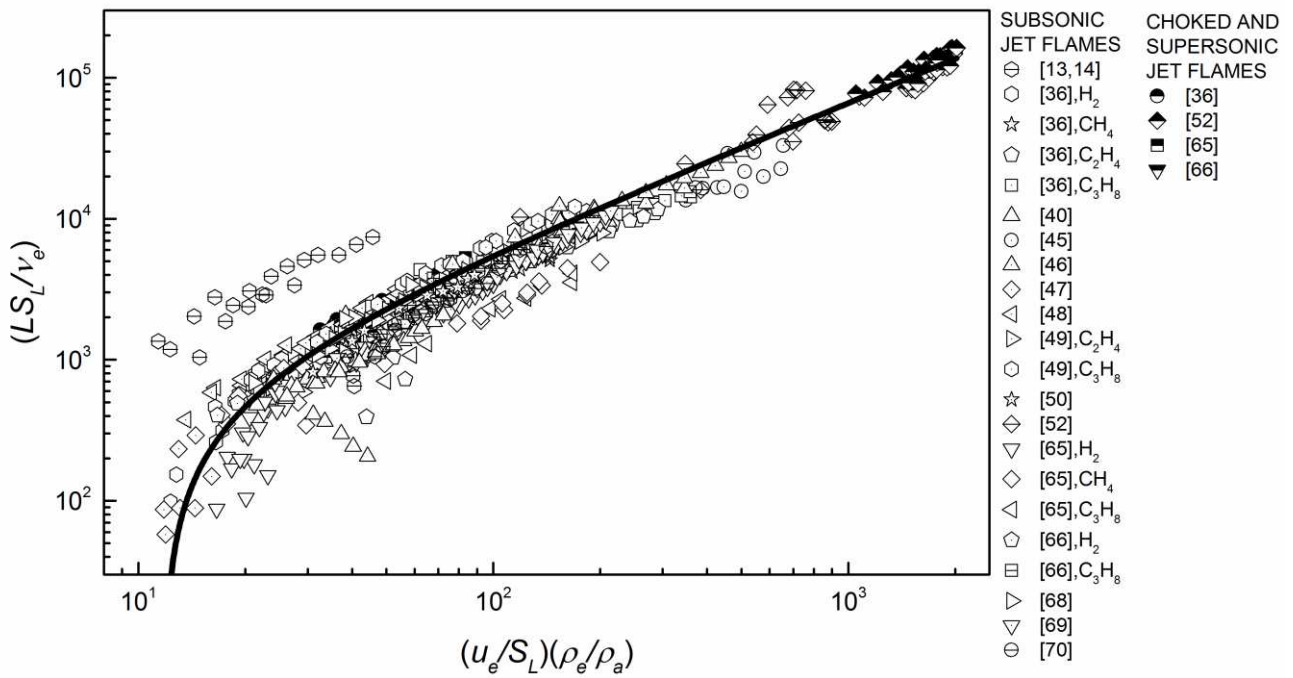Figure 4. Normalised flame height, H/D, as a function of U*. Key to symbols as in Fig. 2.

19

Figure 5. Normalised lift-off distance versus dimensionless flow, with data from present data bank. Correlation of Kalghatgi [36] and Wu et al. [66,67].
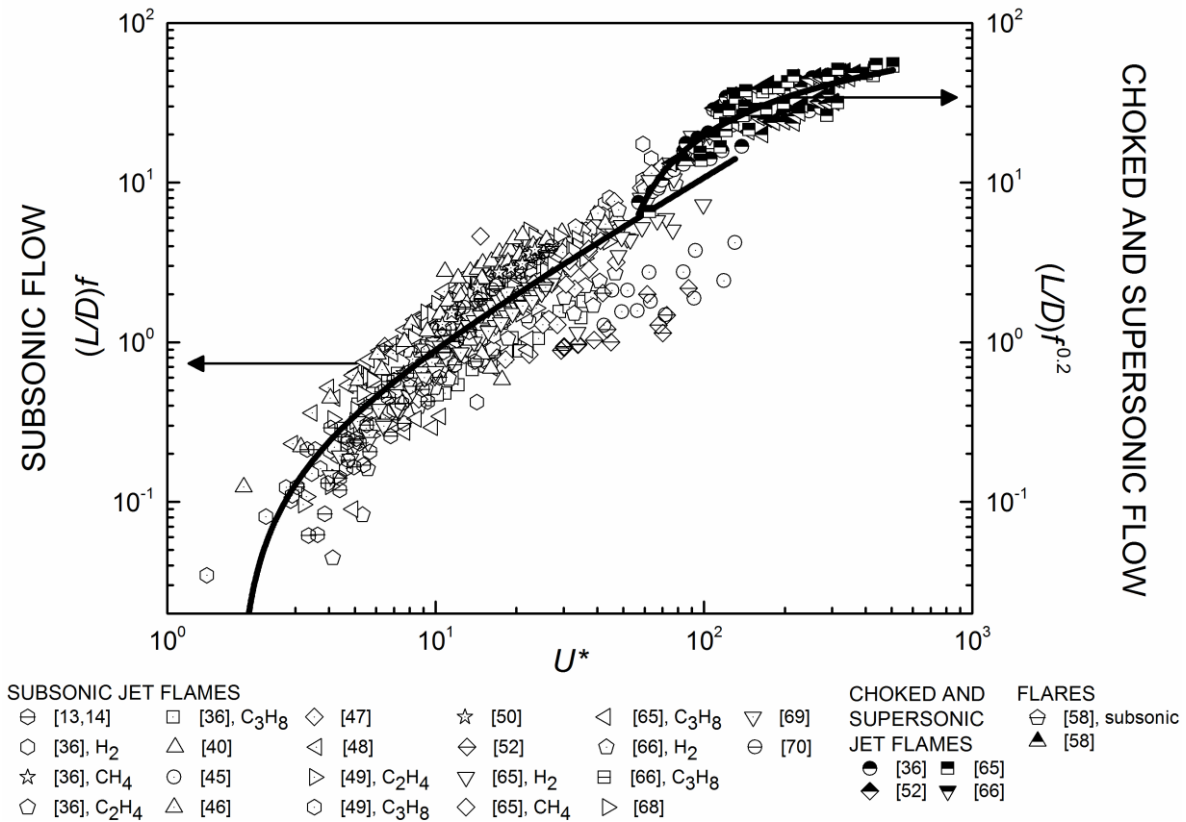

Figure 6. Normalised flame lift-off distances for subsonic (left ordinate) and choked/supersonic (right ordinate) regimes.
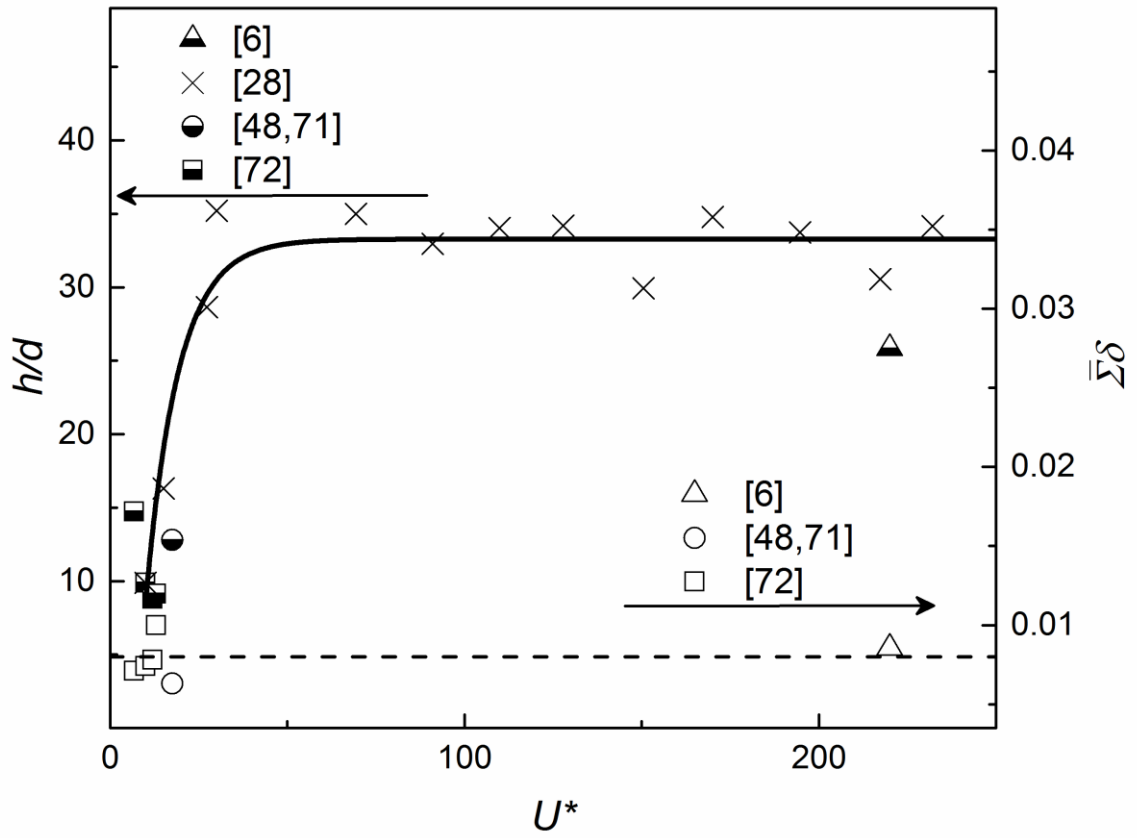
Figure. 7. Derived radiant emitting plume flame heights, h/d, and $\left(\overline{\varSigma\delta}\right)$ as a function of U* for a range of jet flames.

List of Figure Captions

Figure 1. Infra-red image [28] of a propane jet flame, flame height, H, the lift-off distance, L, length of radiant emitting plume, h, and pipe exit plane, diameter D.

Figure 2. Normalised flame height, H/D, as a function of $Q^{*2/5}$, from present data bank. Original correlation of McCaffrey [3] shown by bold curve. This terminates at $Q^* = 13 \cdot 10^6$.

Figure 3. Location of mean volumetric heat release rate, related to (a) streamlines, (b) contours of mean mixture fraction, and (c) mean strain rate, s^{-1}, u = 100 m/s and D = 9 mm. From [5]. The pipe diameter, D, is shown as d in the figure.

Figure 4. Normalised flame height, H/D, as a function of U*. Key to symbols as in Fig. 2.

Figure 5. Normalised lift-off distance versus dimensionless flow, with data from present data bank. Correlation of Kalghatgi [36] and Wu et al. [66,67].

Figure 6. Normalised flame lift-off distances for subsonic (left ordinate) and choked/supersonic (right ordinate) regimes.

Figure. 7. Derived radiant emitting plume flame heights, h/d, and $\left(\overline{\Sigma}\delta\right)$ as a function of U* for a range of jet flames.